

VI

Aqua Reticulata: topology of liquid water networks

Stephen T. Hyde

Department of Applied Mathematics, Research
School of Physical Sciences, Australian National
University, Canberra, A.C.T. 0200, Australia.
stephen.hyde@anu.edu.au

Introduction

Almost 80 years have elapsed since Bernal and Fowler explored the notion of structure at the atomic scale in liquid water.¹ While not the earliest attempt to explain the physical anomalies of liquid water, the work remains a firm starting point to rationalise the structure of liquid water as a function of temperature. At last count, these number more than sixty distinct anomalies,² e.g. melting and boiling temperature, density, compressibility and specific heat variations with temperature.³ Two related principles, both deduced from relatively primitive X-ray scattering studies of water, were articulated in Bernal and Fowler's paper. First, water has a tendency to form networks with tetrahedral symmetry. The net edges are hydrogen-bonded $O \cdots H - O$ units, branched at oxygen vertices (the net nodes), with four edges at each vertex. Second, liquid water is a mixture of two distinct structural forms of low and high density, whose proportions vary on heating or cooling. The lower density form was related to silica polymorphs, namely tridymite (structurally equivalent to the Ice I_h , the most common form of ice at ambient pressure) and quartz. (Later, following the discovery of a new intermediate silicate phase (keatite), Bernal

suggested this silicate phase as a better water analogue.⁴) He proposed that on heating, liquid water approaches the structure of more common ideal liquids (such as metallic melts), and adopted a cubic close-packed model for the high-density form. Eventually, Bernal rejected that “two-state” model as being too crystallographic, and focussed instead on structural features of random networks, or “heaps”,⁴ whose local coordination was approximately tetrahedral, initiating the field of statistical geometry. In this model, he assumed that liquid water is a single homogeneous “continuum” material rather than a mixture, similar to more recent descriptions of packed granular materials such as sand piles. Like conventional covalently bonded crystals, heaps can be described as nets, albeit geometrically disordered, given some criterion for the presence of edges linking pairs of grains (e.g. minimum separation).

Since Bernal’s time, the rise of numerical simulations, and the development of synchrotron and neutron scattering as well as other experimental techniques, has seeded newer models. Variants of the two-state model have been repeatedly proposed, characterised by states of relatively lower and higher density, (see, for example,^{2,5}) and the putative presence of smaller polymolecular water clusters, floating in a sea of more or less disconnected molecular species. Further, the formation of water “strings” in the liquid state has been proposed on the basis of absorption spectroscopy data,⁶ since disputed.⁷ It is somewhat sobering to realise that despite the central importance of water structure, our picture of the structure of liquid water remains unresolved. Evidence supporting these structurally distinct models: multi-state, string and continuum are still inconclusive.

A part of that apparent confusion surely lies in the various techniques used to probe “water structure”. Distinct techniques from X-ray and neutron scattering, to X-ray Raman (XRS), x-ray absorption (XAS) and x-ray emission spectroscopy (XES) sample widely disparate time and length scales. It is agreed that fluctuations in local structure are

very rapid. For example, protons freely shuttle back and forth between adjacent oxygen atoms, flipping hydrogen bonds from $O \cdots H - O$ to $O - H \cdots O$, probably occurring at the picosecond time scale. In the analysis below, we ignore those small-scale temporal and spatial fluctuations, to construct a “zeroth-order” model, that averages over macroscopic volumes and very short time scales, corresponding to the effective structure sensed by scattering studies (that probe a macroscopic water sample at attosecond time scales). The model is strictly topological in scope, without appeal to physics or chemistry. I am interested in exploring what can be concluded about liquid water in the absence of any underlying hypotheses of geometric, chemical or physical nature. We shall see that this bold mission is in fact impossible. To arrive at some structural predictions then, I introduce some (and as little as possible) metric data, namely $O \cdots H - O$ distance data and surface to volume ratios of tessellating surfaces.

Here I revisit Bernal’s original hypothesis in the light of more recent data. My primary goal is to construct as simple a model as possible that is consistent with current data. I emphasise that this analysis cannot clarify the “higher order” models guiding debates around local spatial and temporal fluctuations in bulk water. Hopefully, however, it can afford a simple foundation on which more refined decorations must rest.

How does this analysis relate to the topic of the celebrated debate between Galileo Galilei and his adversary Ludovico delle Colombe? I will not address the central issue of the debate: why these densities adopt their relative values in crystalline and amorphous states. Rather, the analysis outlined in this article relies on accurate density data as an input to deducing the network structure of liquid water. In my view, it is crucial to deduce a firm picture of the structure of liquid water before engaging in the original debate topic. Therefore, this contribution wrestles with that (difficult) preamble to the debate only.

2 Current best data on local structure of water

Scattering studies of liquid water are useful probes of bulk water liquid structure. The technique differs little from the earliest efforts to understand liquid water via X-ray diffraction by Bernal, a pioneering crystallographer without peer. Scattering methods cannot tell us the actual geometry of the arrangement of water molecules in the liquid state, due to the absence of long-range geometric order. However, they allow reconstruction of the atomic two-point correlation function (or radial density function, “rdf”) between pairs of hydrogen and oxygen atoms in the sample – a coarse, but somewhat helpful structural measure.

Most recently, Skinner and colleagues have collected and analysed an impressive suite of scattering data collected from synchrotron radiation.⁸ Reconstruction of the water rdf is significantly better than previous efforts, due to instrumental advances. Data was analysed from a range of different water samples (both confined and unconfined) from -38° - 100°C .⁹ In order to obtain $g(r)_{\text{O-O}}$ between oxygen atoms alone, the H – H and O – H contributions must be subtracted. Here, additional data is required, as direct probes of O and H contributions to the synchrotron scattering are impossible. Skinner *et al.* use neutron scattering data, arriving at a concise estimate of $g(r)_{\text{O-O}}$. The analyses reveal a linear dependence of the (spatially average) O · · · H – O distance in liquid water, between 2.795\AA at 0° and 2.827\AA at 100° , viz.:⁹

$$d(\text{O} - \text{O}) = 0.00032T + 2.7954 \quad (1)$$

where $d(\text{O} - \text{O})$ is the inter-oxygen spacing in \AA and T is the temperature ($^{\circ}\text{C}$).

Integration of $g(r)_{\text{O-O}}$, to give the number of O atoms coordinated to a central O, revealed an isosbestic crossover at $d(\text{O} - \text{O}) = 3.32\text{\AA}$ at all temperatures, with a coordination number of 4.3.⁹ They propose this distance then as characteristic of the first coordination shell of

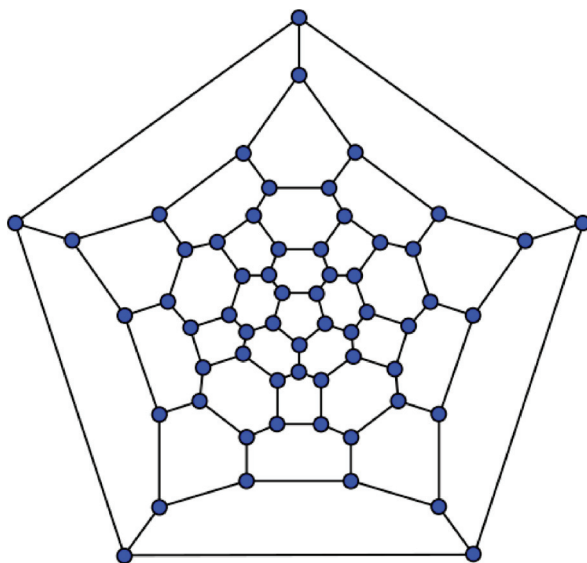


Figure VI.1. The C_{60} net (tic in Ref. 11) drawn as a Schlegel diagram in the two-dimensional euclidean plane, via (for example) stereographic projection from the net on the sphere to the complex plane. The two-dimensional rings of C_{60} are 5- and 6-rings only.

O atoms in the average water liquid structure, whose dimensions are fixed between melting and freezing. This assumption is arguable, given that the van der Waals radius of O atoms is 1.55\AA , implying that O atoms that are not H-bonded are also counted within the first coordination shell (also going some way to explain the fact that the coordination number exceeds 4, that of an ideal tetrahedral liquid). It is however a useful working assumption for further analysis. Indeed, from additional identification of the second “coordination shell”, the authors deduce O–O–O angles that are very close to the ideal tetrahedral angle (109.5°), varying between $108 - 112^\circ$.⁹

This data offers firm support then for Bernal’s original structural hypothesis: that liquid water is a tetrahedral network, at least averaged

over macroscopic volumes. In our topological analysis that follows, we adopt the simpler assumption that liquid (and crystalline) water is a network with (on average) four H-bonded neighbours around each O atom. From a topological perspective, a network is a spatial embedding (in our case in three euclidean dimensions) of a graph, a suite of connected edges and vertices with neither placement in space nor metric extent. Further, the location of the H atom between H-bonded O atoms (i.e. $O \cdots H - O$) assigns a direction to each edge, so the water network is a directed graph at any instant, with, at least on average, two incoming and two outgoing edges linked to each O vertex within the graph. The edge directions are relevant to liquid water physics, but we ignore them here, and consider only the undirected graph, which we assume is a degree-four graph (averaged over all vertices), corresponding to the four edges emanating from each vertex. Here I use the term “graph” to denote the topological structure of a network and “net” the spatial embedding of the graph (adopting, loosely the terminology in Ref. 10, with the exception that “nets” here can be geometrically ordered and crystalline, or disordered).

2.1 Two and three-dimensional rings in a net embedded in three-dimensional space

The graph topology is captured, in part, by its ring structure. In an infinite network (e.g. the ideal network of Ice I), cycles with arbitrarily large numbers of vertices are formed. There is, however, a minimal set of smallest rings whose union defines the entire net. “Strong rings” have been defined for periodic graphs embedded in three spatial dimensions via tilings, by O’Keeffe and colleagues.¹⁰ However, this set of cycles (which are the three-dimensional rings) includes strong rings whose edges are also contained in more than one other ring, giving closed, polyhedral three-dimensional “tiles”. We prefer to

exclude those redundant rings, giving a minimal set of rings, such that each edge is common to only two rings. One way to detect those rings is to find an oriented 2-manifold (a two-dimensional surface) able to support a reticulation whose topological structure is that of the graph. This construction is clear in the case of simpler finite nets that form reticulations of the 2-sphere. Think, for example, of the degree-3 net of sp^2 carbon atoms in the fullerene C_{60} . Cycles can be found in the net with up to 20 vertices, but the net sits in the two-dimensional sphere such that all cycles can be made up of sums of edges of the elemental 5- and 6-rings in the net (see Figure VI.1). We intuit a 2-sphere embedding of the buckminsterfullerene net, since the smallest cycles in the net form a reticulation of that 2-manifold. An underlying manifold for more complex nets is often less evident, and two-dimensional geometry, which classifies 2-manifolds according to its topological genus and underlying Gaussian curvature, offers a useful guide.

For example, the graphene net (**pbz**) is often described as planar, since it reticulates the usual two-dimensional euclidean plane. (For convenience, I label nets and their underlying topological graphs by a three-letter code in **bold script** from the RCSR catalogue)¹¹ Since this net has three hexagons around each vertex, we describe it by the two-dimensional vertex symbol (6.6.6). The two-dimensional vertex symbol encodes in cyclic order the ring-sizes of all the faces that share a vertex in the net. In contrast, the fullerene C_{60} net (**tic**), with vertex symbol (5.6.6), reticulates the two-dimensional sphere. If 8-rings are inserted into the graphite network, giving a net with vertex symbol (6.8.8), the resulting net reticulates hyperbolic 2-manifolds, with negative Gaussian curvature (in place of the zero and positive Gaussian curvature characteristic of the plane and two-dimensional sphere respectively). Examples, reticulating the G, D and P triply periodic minimal surfaces, can be found on-line (at epinet.anu.edu.au/sqc12886, epinet.anu.edu.au/sqc9271 and epinet.anu.edu.au/sqc9265 respectively).

All three crystalline nets are derived from a single underlying hyperbolic (6.8.8) net (*epinet.anu.edu.au/UQC19*). This hyperbolic, two-dimensional picture of crystalline nets is at first encounter an odd way to describe these structures, that are, after all, three-dimensional crystals. For example, the **pbz** net (see *rcsr.anu.edu.au/nets/pbz*), a novel form of graphite, is more conventionally described as a cubic array of twisted 6-rings, arranged in a three-dimensional lattice. But this net topology is exactly reproduced by the (6.8.8) reticulation of the D-surface, mentioned above.

Like the plane and sphere, the D-surface is a two-dimensional space, or a 2-manifold. König's Theorem guarantees that we can find a 2-manifold for any net. More accurately, the theorem asserts that any connected graph may be embedded in an orientable surface to form the edges and vertices of a map.¹² A map is a set of simply-connected regions (faces on the surface), bounded by the edges and vertices of the graph. Note that a face may have a single edge that appears more than once on its boundary, in which case the face winds surrounds a channel of the surface. Given that possibility, the theorem is almost trivial, since for any graph we can form a map simply by inflating all edges to tubes, and merging the tubes smoothly, to give a sponge-like (and almost inevitably hyperbolic) surface, with one tube per graph edge. That embedding has just one face, with ring-size equal to the total number of edges on the graph. In general, however, this is a redundant embedding, with far more tubes, and far larger faces, than necessary. Among the various possible two-dimensional embeddings for the net, we choose the minimal embedding,¹³ with the simplest topology among all oriented surfaces. (Note that here the term "minimal" refers to the surface genus, and is unrelated to "minimal surfaces", discussed below.) This topological constraint is a sensible one, since it implies (via Euler's formula, below) that we find the set of smallest faces, or two-dimensional rings. That choice is equivalent to fitting an oriented 2-manifold through the three-dimensional net such that it passes through all net nodes and edges, and maximises the two-

dimensional density of nodes in the manifold (the number of nodes per unit area). (This two-dimensional density is distinct from the three-dimensional density.) For example, a graph of edges of the tetrahedron can be embedded on a tubular surface with three channels emerging from all four distinct nodes, and meeting up to form a tubular surface whose tubes lie on edges of the tetrahedron. That embedding (which is maximal) is on a genus-two surface, with one face of ring-size equal to the number of edges, six (and two-dimensional vertex symbol (6)). In contrast, the minimal embedding is on the genus zero sphere, with four triangular faces (with two-dimensional ring-size equal to three, and two-dimensional vertex symbol (3.3.3)). In general, the detection of the (minimal, oriented) 2-manifolds for an arbitrary infinite net, crystalline or disordered, is a difficult problem. (The inverse problem, to enumerate infinite crystalline nets as reticulations of 2-manifolds, forms the basis of the *Epinet* project.¹⁴) The net topology software *Topos* can, in many cases, detect 2-manifolds that support infinite crystalline nets and offers a useful route,¹⁵ though the full power of this numerical approach requires further exploration. In general, the minimal manifold is not unique. However, in some cases, we do know the 2-manifold minimal embedding. A fuller description of some known examples can be found elsewhere.¹⁶ In general, the two-dimensional rings are a subset of the rings described by the extended three-dimensional vertex symbol.¹⁷ They are also a subset of the rings that describe faces of the three-dimensional tiling, introduced by O’Keeffe (Ref. 10 and listed on-line at rcsr.anu.edu.au/nets).

The relationship between two- and three-dimensional rings is clear for simpler infinite nets. For example, in the **sod** net (the aluminosilicate skeleton of the zeolite sodalite, rcsr.anu.edu.au/nets/sod) a subset of the three-dimensional rings lie in the 2-manifold, forming the two-dimensional rings, while the remaining three-dimensional rings form “collars” around channels of the manifold. The three-dimensional ring symbol (the vertex symbol) for **sod** is (4.4.6.6.6.6).¹⁷ If a pair of 4-rings sharing a common vertex (and no edges) is selected

as collar rings, the P surface emerges as the support surface, and the two-dimensional rings are the remaining rings, giving two-dimensional symbol (6.6.6.6) (as illustrated at epinet.anu.edu.au/UQC3); selection of a pair of 6-rings as the collars results in the minimal embedding on the D surface, with two-dimensional symbol (4.6.4.6) (illustrated at epinet.anu.edu.au/UQC4). (Here just one symbol describes all vertices, since they are topologically equivalent in the **sod** net.). In fact, a number of embeddings of hyperbolic nets on minimal surfaces give the **sod** net, as shown at epinet.anu.edu.au/sqc970. The minimal embedding for sod is the (4.6.4.6) reticulation of the D-surface, since this has the smallest average two-dimensional ring-size. A more detailed discussion of this issue can be found at Ref. 18.

It is useful to introduce an average two-dimensional ring-size,

$$\langle n^{(2)} \rangle := \frac{\sum_i z_i}{\sum_j \frac{1}{n^{(2)}_j}}$$

where \sum_i denotes the sum over all net vertices, and \sum_j the sum over all z_i two-dimensional rings that share vertex i . So, if the two-dimensional vertex symbol for a degree-four net is (n_1, n_2, n_3, n_4) ,

$$\langle n^{(2)} \rangle := \frac{4}{n_1^{-1} + n_2^{-1} + n_3^{-1} + n_4^{-1}}$$

(so that, for example, $\langle n^{(2)} \rangle = 24/5$ for the (4.6.4.6) minimal embedding of **sod** discussed above. Values of $\langle n^{(2)} \rangle$ for various silicates can be taken from earlier work.¹⁶ Note that the estimated values of $\langle n^{(2)} \rangle$ for keatite (**lon**) and coesite (**coe**) are unknown, however, they can be bounded above and below from the face-sizes in the tilings of these nets.¹¹ Keatite (**kea**, described at rcsr.anu.edu.au/nets/kea) has three-dimensional rings (5.5.5.7.8.8) (4 x multiplicity per unit cell) and (5.7.5.7.5.7) (8x multiplicity). Likely two-dimensional ring symbols are therefore ((5.5.5.7) (4x) and (5.7.5.7) (8x), where the first vertex

type is assumed to have larger 8-rings surrounding channels (collar rings). The two-dimensional ring-size is then:

$$\langle n^{(2)} \rangle = \left(\frac{4.8}{5^{-l} + 5^{-l} + 5^{-l} + 7^{-l}} + \frac{4.8}{5^{-l} + 7^{-l} + 5^{-l} + 7^{-l}} \right) \cdot (12)^{-l} = 5.68$$

Similarly, the three-dimensional rings of the rings of the **coe** net (*rcsr.anu.edu.au/nets/coe*) have symbol (4.8.4.9.6.8) and (4.6.4.6.8.9). The two-dimensional ring-sizes are therefore bounded below by (4.8.4.9) and (4.6.4.6) and above by (4.9.6.8) and (4.6.8.9), corresponding to an average two-dimensional ring-size, $\langle n^{(2)} \rangle$ within the interval [5.12, 6.13]. (I have used the notation $\langle n^{(2)} \rangle$ to emphasise that this refers to the two-dimensional measure of ring-size, which excludes all rings except those that bound faces that tile the underlying 2-manifold. This is distinct from the usual three-dimensional ring-size, which includes collar-rings and other cycles whose homotopies are more complex than the (null homotopic) cycles contributing to $\langle n^{(2)} \rangle$).

3 Silicate network polymorphism

Water and silica are the dominant chemical species on the earth's surface. They share structural features: for example, both typically form tetrahedral networks. It is often stated that – like framework silicates – water exhibits an unusual degree of structural flexibility, evidenced by the wealth of ice phases formed at low temperature under pressure. However, its polymorphism pales in comparison to silicates. While less than twenty phases of ice are known, over a hundred distinct crystalline (alumino-)silicate frameworks are recognised and catalogued.¹⁹

Silicates can form zero-, one-, two-, or three-dimensional nets, according to the number of independent translations vectors that define their structure. Three-dimensional “framework” (or “tecto”) silicates are conveniently sorted into three classes, according to their three-dimensional framework density: “dense”, “intermediate” and “rare” (Table 1).

Table 1: Tetrahedral silicate networks, listed according to their idealised density, from dense silicates to low-density zeolite frameworks (all assumed to have stoichiometry SiO_2). Density and ring-size parameters are defined in the main text.

class	examples	net ID	density, ρ_g	topological density, TD_{10}	2d ring size, $\langle n^{(2)} \rangle$
<i>dense</i>	coesite	coe	869	1318	5.12-6.13
	α -quartz	α-qtz	790	1231	6
	keatite	kea	746	1225	5.68
	β quartz	β-qtz	686	1231	6
	tridymite	lon	666	1027	6
	amorphous silica		660		
<i>intermediate (clathrasils)</i>	melanophlogite	mep	580	1058	5
<i>rare (zeolites)</i>	sodalite	sod	530	791	4.80
	analcime	ana	570	933	4.80
	gmelinite	gme	450	694	4.57
	zeolite ZK-5	kfi	450	681	4.57
	Linde Type-A	lta	430	641	4.80
	zeolite rho	rho	430	641	4.36
	faujasite	fau	380	579	4.36

The physical density of framework silicates is a measure that often depends on the presence of interstitial or intra-framework species and partial substitution of silicon atoms by aluminium or other cations in the framework, as well as variable degrees of framework collapse on dehydration. In order to compare silica with water polymorphs,

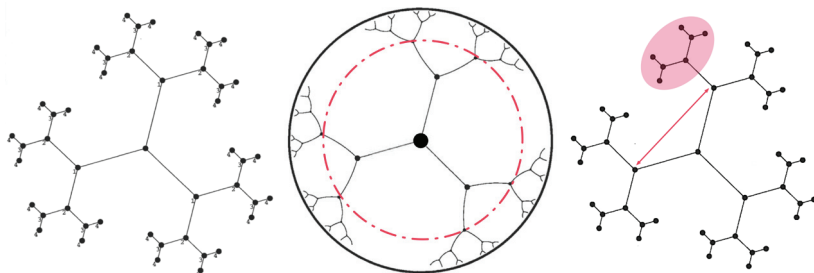


Figure VI.2. (a) A fragment of a degree-three tree. Vertices of the tree are labelled with integers corresponding to the number of edges between the central (origin) node of the tree and those vertices. Shells within the tree fragment are formed by the set of all vertices with equal indices. (b) Embedding of the degree-three tree in the (Poincaré model of the) hyperbolic plane, such that all edges are of equal length, and the tree is regular with symmetrically identical vertices and edges. Vertices in equivalent shells now lie on the perimeters of hyperbolic circles. (One shell is indicated by the dashed circle.) (c) Formation of a three-ring in the tree by fusing the arrowed tree vertices. Closure of an n -sided ring is accompanied by pruning of all vertices in one branch beyond one vertex in shell $\lfloor n/2 \rfloor$ (where $\lfloor \cdot \rfloor$ denotes the integer part of the fraction).

consider an idealised silicate net, with silicon atoms at net nodes, and oxygen anions at mid-edges. We therefore consider the hypothetical net, containing only tetrahedral atoms at nodes, in its fully expanded form, realised by the most symmetric, barycentric embedding of the net topology.²⁰ A dimensionless measure of the geometric net density,

$\rho_g := 10^3 \frac{v l^3}{V}$ where v is the number of tetrahedral nodes in the volume V , and l is the length of net edges (which are generally all equal in the maximally symmetric and least dense form).

Table 1 shows a general trend of increasing (three-dimensional) density with increasing ring-size. This correlation, at first glance counter-intuitive, nevertheless emerges naturally within a two-

dimensional perspective by the following argument (adapted from the original discussion of Bukowinski *et al.*²¹). First, we define a measure of three-dimensional density that is independent of the geometry of the net: the topological density. This number is formed from a decomposition of the net into topological “shells”, formed as follows. Each vertex is labelled with an index, ν_i , equal to the number of edges in a shortest path traversed from that vertex back to a vertex (ν_0) assigned as the origin. The net is thus layered into concentric shells containing the set of vertices with $\nu_i = 0, 1, 2, 3, \dots$, and the number of vertices in each successive shell, N_i , forms an integer coordination sequence.²² Figure VI.2(a) illustrates this construction for a degree-three tree. We define the topological density as:

$$TD_{10} := \sum_{i=0}^{10} N_i$$

The maximum possible topological density results from a (degree- z) net that is a tree, i.e. with no closed cycles, since then each node in the net acts a source for $z - 1$ nodes in the next shell, giving a topological density,

$$TD_S = \frac{S(z - 2) + ((z - 1)^S - 1)z}{z - 2}$$

which grows exponentially fast with the maximum shell number S .

Exponential growth is consistent with the growth of shell perimeter with radius, itself exponential if the shells form a series of concentric circles of linearly increasing radius in the hyperbolic plane (H^2). This conflation of a topological feature, namely the topological density, with metric dimensions is a loose one, but qualitatively exact if one embeds the net such that all edges have equal length, in which case a tree indeed reticulates H^2 (Figure VI.2(b)).²³

The formation of a cycle in the tree involves the pruning of all vertices from the tree due to a root vertex in the cycle, since that root

vertex is “grafted” onto another vertex to form the closed cycle (Figure VI.2(c)). The smaller the ring, the closer to the origin of the net the root vertex lies, so the larger the number of vertices pruned from the tree to form the net. Conversely, large rings lose fewer vertices during this pruning and grafting operation. This argument explains qualitatively the paradoxical direct correlation of topological density with ring size in a net.

In order to derive a quantitative correlation, consider the embedding of the net in a 2-manifold, such that each vertex occupies an (assumed constant for simplicity) area of Ω in the surface. From differential geometry, we can express the geometric density, ρ_g , defined above, in terms of the net topology, via the degree of the vertices (the bond valency), z and the two-dimensional ring-size of the net, $\langle n^{(2)} \rangle$. The

geometric density $\rho_g = \frac{A}{\Omega V}$ where A is the area of the 2-manifold

within volume V . The Gauss-Bonnet Theorem allows us to express A in terms of the surface-average of the Gaussian curvature of the

manifold over area A contained within the volume V , $\langle K \rangle := \frac{\iint K da}{A}$

namely $A = \frac{2\pi\chi}{\langle K \rangle}$, where χ is the Euler-Poincaré characteristic of the

portion of the surface contained within volume V . The geometric density can then be rewritten in terms of a dimensionless surface-to-

area measure, the “homogeneity index”, $h := \frac{A^{3/2}}{(2\pi|\chi|)^{1/2} V}$

The geometric density is then: $\rho_g = \frac{h}{\Omega^{3/2}} \left(\frac{2\pi|\chi|}{V} \right)^{1/2}$.

The final form of the density relation follows from Euler’s formula,

which relates the characteristic χ to the net topology as follows. The usual form of Euler's formula is $\frac{\chi}{v} = 1 - \frac{e}{v} + \frac{f}{v}$ where v , e and f denote the number of vertices, edges and faces (bounded by the two-dimensional rings with size $\langle n^{(2)} \rangle$ of the net in the volume V . But $\frac{e}{v}$, the number of edges emanating from a single vertex, is equal to $z/2$, since each edge is associated with a pair of vertices. Likewise, $\frac{f}{v}$ is equal to $\frac{z}{\langle n^{(2)} \rangle}$ since each vertex contains $\frac{1}{\langle n^{(2)} \rangle}$ of each of the z rings around that vertex. Euler's formula can then be rewritten in terms of the net topology only, viz.:¹⁶

$$\rho_g = \frac{h}{\Omega^{3/2}} \left(\frac{\pi \left((z-2) \langle n^{(2)} \rangle - z \right)^{1/2}}{\langle n^{(2)} \rangle} \right)$$

In keeping with the paper's focus on topology to the exclusion of geometry (as far as possible), we prefer to discuss topological density (TD_{10}) in preference to the geometric density measure ρ_g . This measure of density correlates well with geometric density as shown in Figure VI.3. Indeed, the correlation holds from the least dense framework silicate (faujasite, **fa**) to the densest tetrahedral silicate polymorph, coesite (**coe**), with an approximate relation:

$$TD_{10} = k\rho_g \text{ and } k \approx 1.58 \text{ for the silicate data of Figure VI.3.}$$

It makes sense, then, to recast the issue of geometric structure, and derivative quantities, including geometric density, in terms of topological measures alone. We can write a "normalised" topological density as:

$$TD_{10} = k \frac{h}{\Omega^{3/2}} \left(\frac{\pi \left((z-2) \langle n^{(2)} \rangle - z \right)^{1/2}}{\langle n^{(2)} \rangle} \right) \quad (2)$$

This equation describes surprisingly well the variation of topological density with two-dimensional ring-sizes, with a single parameter, $c := k \frac{h}{\Omega^{3/2}} = 524$, as shown in Figure VI.4. Though possibly treasonable, it is nevertheless not unreasonable to claim that the very simple picture sketched here, of three-dimensional chemical networks as two-dimensional reticulations of hyperbolic manifolds is a valid first-order approximation.

Three parameters influence the magnitude of the topological density: the scaling between topological and geometric densities, k , normalised surface-to-volume ratio, h , and the area in the 2-manifold occupied by each vertex (i.e. SiO_2 group), Ω . The silicate density data suggests that k is constant. The fraction $\frac{h}{\Omega^{3/2}}$ is therefore also

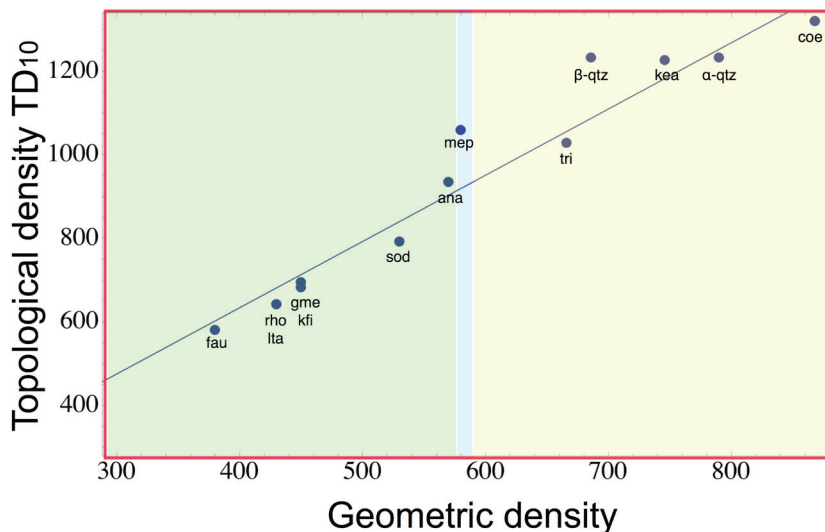


Figure VI.3. Topological vs. geometric density for a number of degree-four (tetrahedral) silicate nets. Polymorphs are labelled by their three-letter net code from Ref. 11 and split into three regions: zeolites, clathrates and dense silicates, listed in Table 1.

approximately constant for the range of silicates, from rare zeolites to the dense frameworks. The value of h is dependent on the geometry of the 2-manifold and its embedding in three-space. The simplest hypothesis is that these 2-manifolds, like those for many zeolites, are in fact 3-periodic minimal surfaces, or, simpler still, embeddings of the canonical hyperbolic manifold, one of uniform negative Gaussian curvature in three-space, with zero mean curvature. Differential geometric arguments then imply that $h = \frac{3}{4}$.²⁴ If we assume that this holds for the tetrahedral silicates, the area per silica node, Ω , must also be fixed, regardless of three-dimensional density. In other words, although the three-dimensional density of tetrahedral tectosilicates varies from very porous zeolites to dense coesite, their two-dimensional density remains fixed. That must follow if h is indeed fixed for the 2-manifolds in which the tetrahedral nets are embedded, and close to its value known for some zeolites from their reticulation on three-periodic minimal surfaces (3/4). This question cannot be resolved definitively at present, since we not know the 2-manifolds that give minimal embeddings of denser silicates than the zeolites. In fact, it is certain that melanophlogite (the **mep** net) cannot reticulate an intersection-free hyperbolic surface via a subset of its strong rings.²⁵ This may also be a feature of other dense nets, particularly those with edges lying along axes of three-fold rotational symmetry in their most symmetric embeddings in three-space, such as **dia** and **lon** nets. In those cases, eq. 3 fails, since the embedding is in surfaces with degree-three branch lines, forming cellular complexes rather than 2-manifolds. Alternatively, we could insist the embedding be in a 2-manifold, in which case the embedding may be a map, but one whose faces have edges appearing more than once in their bounding two-dimensional rings (analogous to the maximal embedding of the tetrahedral graph mentioned on p. 150). For example, the **dia** net embeds in the D-surface as a tree, with a single face and unbounded two-dimensional ring-size, so that formally $\langle n^{(2)} \rangle = \infty$.^{24,26} In that case, Euler's formula fails, and so eq. 3 no longer holds.

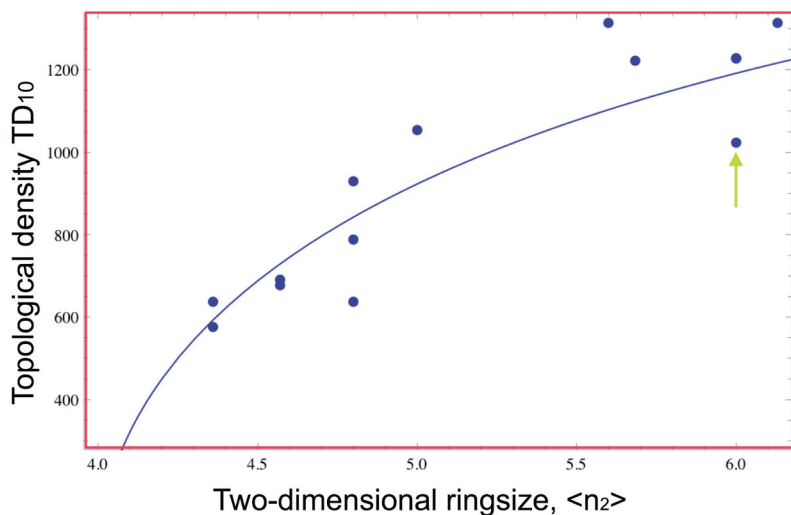


Figure VI.4. Topological density as a function of two-dimensional ring-size for a number of degree-four (tetrahedral) silicate nets. The arrow marks tridymite data. The curve is a best fit to the data via equation 3.

4 Amorphous silica

We can use these fits to infer the simplest topological feature of amorphous or fused silica as follows. Though it is clearly simplistic to suppose that “amorphous silica” is a well-defined polymorph of silica, like the zeolites, clathrates and dense silicates, this assumption is a reasonable one in silicate science, given the characteristic physical properties of amorphous silica. Since it has no geometrically defined crystalline structure, this may seem naïve. However, lack of crystalline (and hence geometric) order, need not imply lack of topological order, to some degree. And the topological analysis developed above can in principle allow us to probe the topological order of fused silica, knowing only its density. Recall, that the analysis is predicated on the notion of a reticulation of a 2-manifold. That picture explains *a priori* the counter-intuitive relation of increasing three-dimensional density

with increasing ring-size inferred from the full range of crystalline tetrahedral polymorphs of silica, from low-density zeolites to dense tectosilicates. Limited simulations of fused silica, inspired by studies of shock-induced densification of fused silica, are consistent with this two-dimensional view. In common with the relation between ring-size and density explained here in terms of 2-manifolds, those simulations also show increasing ring-size on densification.²⁷ Those studies report a (three-dimensional!) average ring-size distribution between 3- and 10-rings, and a significant change in the network topology on densification. In the absence of a full discussion of their ring-size detection algorithm, quantitative comparisons between $\langle n^{(2)} \rangle$ and the ring distributions reported from these simulations are uncertain. Kubota *et al.* write that laser-induced densification of amorphous silica causes a

persistent increase in the 3 and 4-membered rings compared with the unshocked configuration. In addition, the 7- and larger-membered rings also show persistent increases in their contributions to the ring distribution. These persistent changes in the ring coordination indicate the formation of a stable phase of permanently densified fused silica. The large increases observed in the larger rings also suggest the disruption of the fused silica network, and may indicate the existence of cracks, and microvoids. The increases in the smaller strained rings are a plausible connection to the observed permanent densification. The role of the larger rings upon densification is not clear. However the ability for larger rings to exist in compact non-planar configurations suggests that their impact on density is small.

Within a two-dimensional perspective, their report of an increase in large rings (and hence, we suspect, of $\langle n^{(2)} \rangle$) on densification is very reasonable, and consistent with data for crystalline silicates. Indeed, those larger rings are responsible for the densification! The

quote above attempts to write off the influence of large rings, ascribing densification to a very minor change in the number of three-rings, consistent with intuition from a three-dimensional picture. Their results are sensible, their discussion less so. The ring statistics found in simulations form a distribution between 3- and 10-sided rings, peaked between 5- and 6-rings (Figure VI.5).

Their work supports the working hypothesis of amorphous silica as a two-dimensional hyperbolic pattern. Now the density of (relaxed and unshocked) amorphous silica (fused silica glass) is equal to 2.203 g cm^{-3} . It is reasonable to assume that the Si-Si distance in amorphous silica is the same as that of its crystalline counterparts, namely 3.1 \AA , so that the geometric density $\rho_g = 658$. We can then use the linear fit relating geometric and topological density for silicates

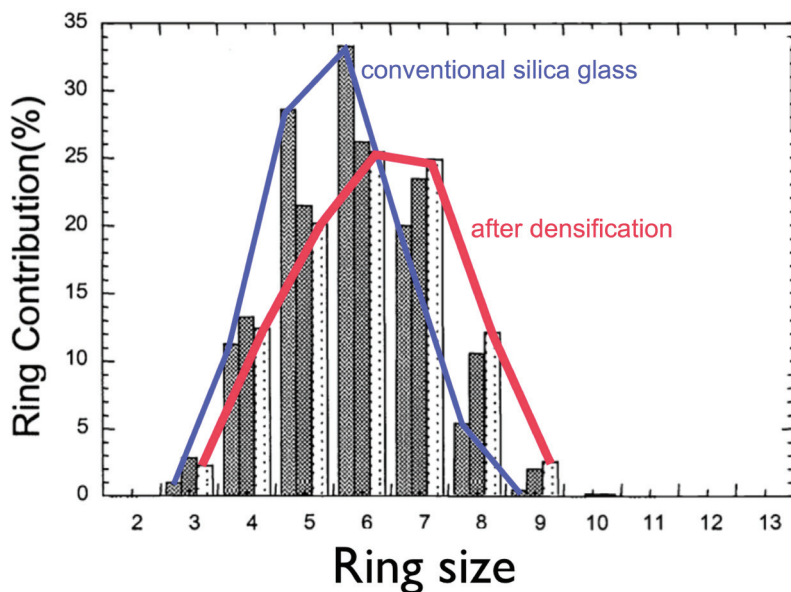


Figure VI.5. Distribution of ring-sizes before, during and after laser-induced densification of amorphous silica, deduced from numerical simulations, adapted from data reported in Ref. 27.

(Figure VI.3) to deduce the topological density, namely $TD_{10} = 1050$. Lastly, eq. 3 (with constant c from the fit shown in Figure VI.4) leads to an estimate of the average two-dimensional ring-size, $\langle n^{(2)} \rangle \approx 5.4$, illustrated in Figure VI.6. Though direct comparison with the ring statistics reported in Ref. 27 is uncertain, this value is close to the average reported by Kubota *et al.* (see Figure VI.5).

These authors also reported a densification of 20% on laser-shock treatment, which (assuming no change in Si-Si distances) implies that the denser phase has topological density $FD_{10} \approx 1150$, realised by a hyperbolic network with $\langle n^{(2)} \rangle \approx 5.8$. This increase too is consistent with the ring statistics reported in Ref. 27 (see Figure VI.5).

5 Ices

The close parallels between silicate and ice frameworks mean that the foregoing analysis that allows an estimate of the two-dimensional ring-size of the amorphous silica framework is easily modified to predict $\langle n^{(2)} \rangle$ for liquid water.

Unfortunately, the wealth of tetrahedral framework silicates is not matched by “pseudo-tetrahedral” ice phases. (I use this term to denote ice/water nets with four edges per node. Typically, the edges radiate from the centre of each tetrahedron to their four vertices. But since the analysis is topological rather than geometric, the edge geometry is irrelevant, and any degree-four network is admissible.) Six distinct pseudo-tetrahedral ice crystalline polymorphs are known. Their structural data are tabulated in Table 2.

Table 2: Tetrahedral ice networks. Density and ring-size parameters are defined in the main text (*cf.* Table 1).

class	examples	net ID	density, ρ_g	topological density, TD_{10}	2d ring size, $\langle n^2 \rangle$
dense	ice II	ict	833	1333	6
	ice III	kea	833	1225	5.68
	ice Ih	lon	637	1027	6
	ice Ic	dia	649	981	6
intermediate (<i>clathrates</i>)	clathrate I	mep	549	1058	5
	clathrate II	mtn	545	1049	5

Like the silicate data, the topological and geometric densities for the ice frameworks are related by $TD_{10} = k'\rho_g$, where a best fit

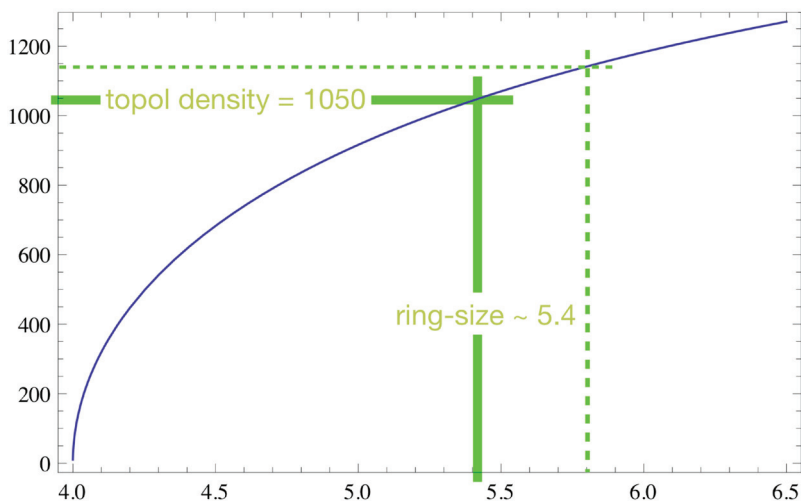


Figure VI.6. Estimate of the two-dimensional ring-sizes of normal and densified amorphous silica from their framework densities (see main text). The data suggests that amorphous silica has a two-dimensional ring-size, $\langle v^2 \rangle \approx 5.4$ (full lines). The dotted lines show the corresponding data for laser-shocked densified silica.

gives $k' = 1.62$ (Figure VI.7). This is slightly larger than the constant k found for silicates, though the difference is insignificant given the scatter of the data.

The limited data also is also consistent with eq. 2, where the best fit is found for $c' = \frac{k' h}{\Omega^{3/2}} = 832$, as shown in Figure VI.8. Again, the paucity of data (compared with silicates) does not allow definitive estimate of the constancy or otherwise of k' . The data are, however, consistent with the functional form of eq. 2 assuming that c' is constant.

6 Liquid water

The density of liquid water at atmospheric pressure has been measured carefully between 0 and 100°C.²⁸ Combining that data with the recently measured $O \cdots H - O$ distances in liquid water (eq. 1) leads to the conclusion that the topological density of liquid water changes only

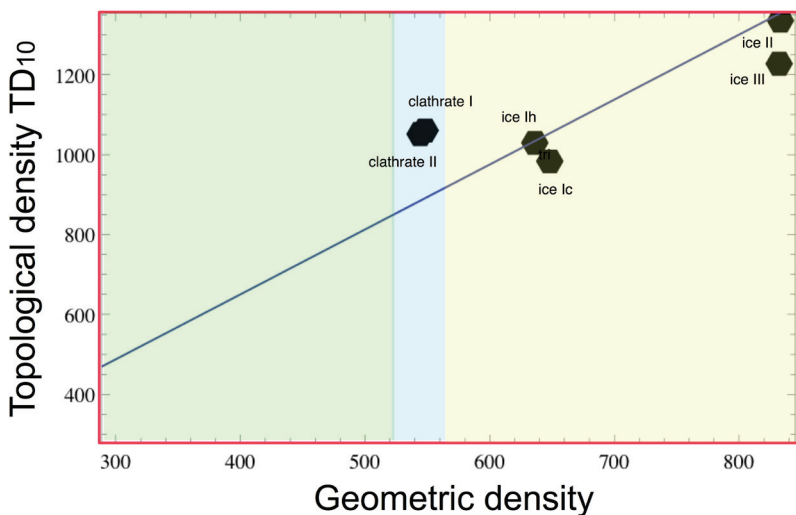


Figure VI.7. Topological vs. geometric density of crystalline pseudo-tetrahedral ice polymorphs (*cf.* Table 2).

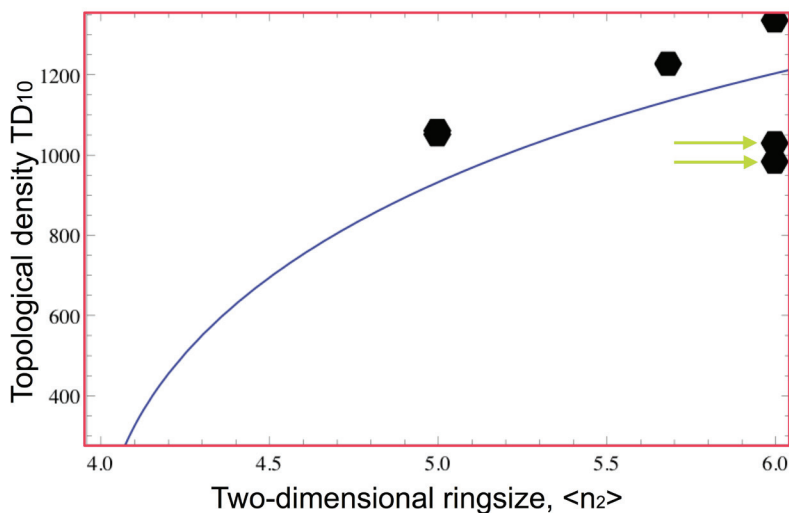


Figure VI.8. Topological density as a function of two-dimensional ring-size for ice polymorphs (*cf.* Figure VI.4.) The arrows mark data for hexagonal and cubic forms of ice I (lower and upper respectively).

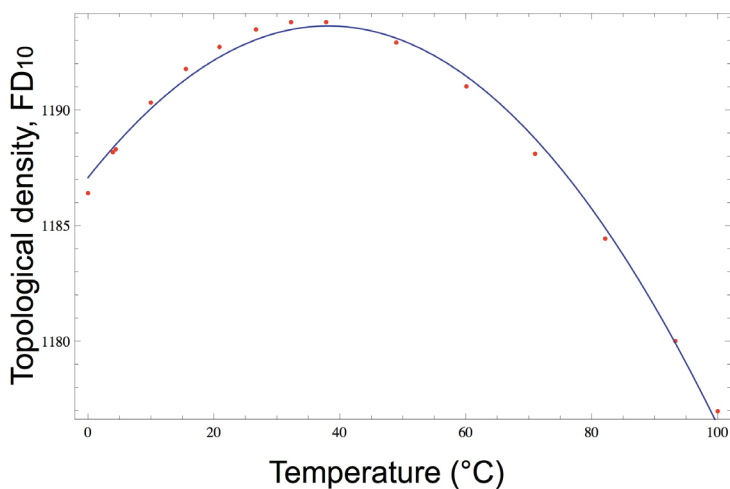


Figure VI.9. Topological density of water, TD_{10} , as a function of temperature at atmospheric pressure.)

marginally (between 1194 and 1176, peaking in density very close to body temperature) over the entire range from 0-100°C, as shown in Figure VI.9.

According to the fit deduced from the ice polymorphs (Figure VI.8), this variation in topological density is accounted for by a variation of the two-dimensional ring-size, $\langle n^{(2)} \rangle$ between [5.83 – 5.88], i.e. varying only very slightly over the complete temperature range up to 100°C, as plotted in Figure VI.10.

7 Closing and an auto-critique

What can be gleaned from this analysis? First, the concept of water as a tetrahedral framework, due to Bernal, remains reasonable. However, his and Fowler's original concept of liquid water as a continuum of states, from relatively open tetrahedral nets at lower temperatures, to denser patterns closer to its boiling point – reminiscent of close-packed structures – is not consistent with the most recent scattering analyses. These data suggest that the (geometric) density variations with temperature are not accompanied by significant changes in topological density, so that the network topology of liquid water is rather constant with temperature. This conclusion also argues against more recent “two-state” models of water, all of which imply measureable changes in water network topology with temperature. In addition, the supposed presence of water “strings” is not supported by this analysis.⁶ Strings have a degree of just two, and the presence of strings would be expected to lower the (average) degree of the bonding net in liquid water, z , below four. In fact, as mentioned in the **Introduction**, scattering studies suggest an average first-shell coordination slightly larger than four.⁸ Further, our analysis suggests that density is expected to increase with increasing z and $\langle n^{(2)} \rangle$ (cf. eq. 2). Since melting of ice is accompanied by an increase in density, were water strings to form (thereby lowering z) a compensating increase in $\langle n^{(2)} \rangle$ (beyond 6)

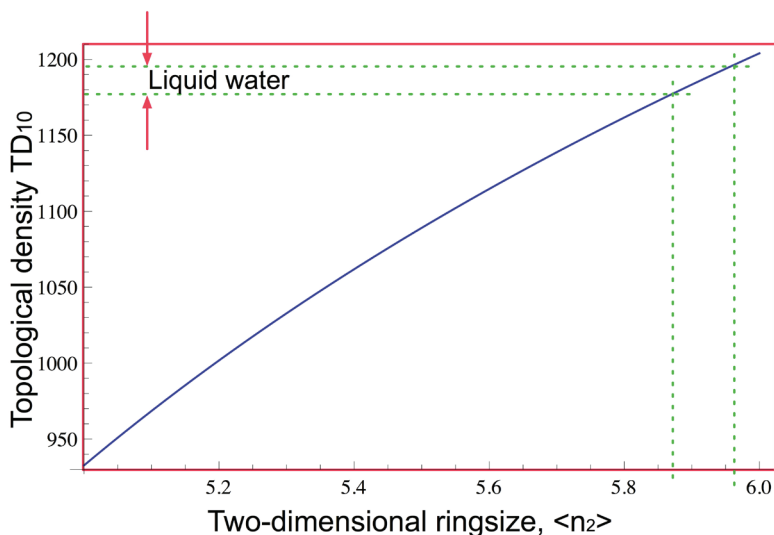


Figure VI.10. Estimate of the two-dimensional ring-sizes of liquid water between 0-100 °C (cf. Figure VI.6).

would be required. For example, if $\langle n^{(2)} \rangle = 6$ and $z = 4$ (corresponding to ice I), the topological density for ice/water (assuming $c' = 832$) is $TD_{10} = 1183$. If z drops to (e.g.) 3.8 to accommodate strings, $\langle n^{(2)} \rangle$ must increase to larger than 6.6 to achieve a denser melt than ice, a severe topological change, for which there is no supporting evidence. Other water models have argued for clathrate-like clusters, forming finite domains (see, for example, Ref. 5). Evidently, finite clusters have $z < 4$, due to the boundary. So here too, large rings are essential to achieve the increased density within the cluster (and still larger to achieve the required bulk density, due to low density interstitial regions between clusters). Such models therefore appear unlikely candidates for liquid water structures, within this two-dimensional view.

This estimate of the two-dimensional ring-size of liquid water is dependent on the assumption that the “constants” linking topological and geometric density (k') and topological density and ring-size (c')

have fixed values for all pseudo-tetrahedral ice polymorphs as well as liquid water. Unfortunately, minimal 2-manifold embeddings for the ice polymorphs are unknown, in common with dense silicate networks. Given that difficulty, I can only estimate the crucial parameters governing the topology of these nets $\langle n^{(2)} \rangle$, h and hence Ω . It is therefore likely that the single topological measure extracted from this analysis, $\langle n^{(2)} \rangle$ for amorphous silica and liquid water, is an approximation only. To go further, more detailed explorations of minimal embeddings of (particularly dense) nets are required.

Reflection on the central issue that drove the original debate between Galileo and delle Colombe reveals the uncertainty in my simple analysis. I have argued that the (topological) density grows with increasing two-dimensional ring-size. How can it be then, that conventional ice (Ic), with $\langle n^{(2)} \rangle = 6$, floats on water $\langle n^{(2)} \rangle (\approx 5.9)$? Inspection of the density-ring-size data (Figs. 4,9) reveals that the topological density for ice I (cubic and hexagonal forms) is substantially lower than that predicted from the best fit for ice polymorphs (see arrowed data points in Figure VI.8). Recall that the topological density depends on ring-size ($\langle n^{(2)} \rangle$ network degree (z), and the constants h , Ω and k (or k'). It is notable that the tridymite polymorph of silica, which also has $\langle n^{(2)} \rangle = 6$ (and is structurally equivalent to ice Ih) is similarly anomalous compared with other silicates, with an unexpectedly low density for its ring-size (arrowed data in Figure VI.4). In the absence of known minimal 2-manifold embeddings for **lon** (tridymite, Ice Ih) and **dia** (ice Ic), this anomaly, common to both amorphous silica and liquid water, remains unresolved. It is likely a central issue surrounding the issue of relative densities of liquid and frozen water. We can, however, conclude that both amorphous silica and liquid water have similar network topologies, namely degree-four nets with average ring-sizes likely between 5.5-6. Further, the density and accompanying ring-size variations between crystalline and amorphous states of water and silica are similar, suggesting that these relative densities may be a

feature of tetrahedral frameworks in general, rather than a peculiarity of H₂O nets.

Perhaps the most valuable aspect of this analysis lies in the topological approach, rather than the quantitative details. Bernal's concept of structural similarities between liquid water and (possibly multi-phase) crystalline silicate networks initiated rigorous discussions of the concept of water structure. While useful, direct analogies with crystalline networks are overly simplistic and misleading. Indeed, the current controversy over two-state models and related crystalline phases appears to have overlooked the potent arguments of Fletcher that the phenomenon of super-cooling of liquid-state water is incompatible with a network that resembles crystalline frameworks. As he wrote in 1971 "*It is clear, from considerations based on the possibility of supercooling water at various pressures, that the liquid does not contain any significantly large fraction of cluster with structure identical with that of one of the ices.*"²⁹ Quantitative investigations and comparisons of ordered and disordered structures require approaches that jettison the usual geometric concepts underlying crystalline patterns. The ideas discussed here are a simplistic attempt to explore structural frameworks at this broader level. They offer a starting point for further investigations.

Acknowledgements

I thank Lawrie Skinner and John Parise for generously sending me their water diffraction data prior to publication.

References

1. Bernal, J. D; Fowler., R. H. *J. Chem. Phys.* **1933**, *1*, 515.
2. Huang, C.; Wikfeldt, K. T.; Tokushima, T.; Nordlund, D.; Harada, Y.; Bergmann, U.; Niebuhr, M.; Weiss, T. M.; Horikawa, Y.; Leetmaa, M.; Ljungberg, M. P.; Takahashi, O.; Lenz, A.; Ojamae, L.; Lyubartsev, A.

- P.; Shin, S.; Pettersson, L. G. M.; Nilsson, A. *Proc. Natl. Acad. Sci. USA* **2009**, *106*, 15241.
3. Chaplin, M. *Anomalous properties of water*. <http://www.lsbu.ac.uk/water/anmlies.html>
 4. Bernal, J. D. *Proc. Roy. Soc. Lond. A* **1964**, *280*, 299-322.
 5. Martin, C. *The icosahedral water clusters*. <http://www1.lsbu.ac.uk/water/clusters.html>
 6. Wernet, Ph.; Nordlund, D.; Bergmann, U.; Cavalleri, M.; Odelius, M.; Ogasawara, H.; Näslund, L.; Hirsch, T. K.; Ojamäe, L.; Glatzel, P.; Pettersson, L. G. M.; Nilsson, A. *Science* **2004**, *304*, 995-999.
 7. Head-Gordon, T.; Johnson, M. E. *Proc. Natl. Acad. Sci. USA* **2004**, *103*, 7973-7977.
 8. Skinner, L. B.; Huang, C.; Schlesinger, D.; Pettersson, L. G. M.; Nilsson, A.; Benmore, C. J. *J. Chem. Phys.* **2013**, *138*, 074506.
 9. Skinner, L. B.; Benmore, C. J.; Neufeind, J. C.; Parise, J. B. A structural description of the compressibility minimum in water. *preprint*, 2013.
 10. Delgado-Friedrichs, O.; O'Keeffe, M. *J. Solid State Chem.* **2005**, *178*, 2480-2485.
 11. O'Keeffe, M.; Peskov, M. A.; Ramsden, S. J.; Yaghi, O. *Acc. Chem. Res.* **2008**, *41*, 1782-1789.
 12. Lindsay, J. H. *Am. Math. Monthly* **1959**, *16*, 117-118.
 13. Firby, P. A.; Gardiner, C. F. *Surface Topology*. Ellis Horwood, New York, 2001.
 14. Hyde, S. T.; Robins, V.; Ramsden, S.. *Epinet*. <http://epinet.anu.edu.au>, **2008**.
 15. Blatov, V. A. *Struct. Chem.* **2012**, *23*, 955-963.
 16. Hyde, S. T. *Acta Cryst. A* **1993**, *50*, 753-759.
 17. O'Keeffe, M.; Hyde, B. G. *Crystal Structures. I. Patterns and Symmetry*, Mineralogical Society of America, Washington D.C., 1996.
 18. Hyde, S. T. in *Defects and Processes in the Solid State. Some Examples in Earth Sciences*, Elsevier, Amsterdam, **1993**.
 19. Baerlocher, Ch.; McCusker, L. B. *Database of zeolite structures*. <http://www.iza-structure.org/databases/>

20. Delgado-Friedrichs, O.; O’Keeffe, M. *Acta Cryst. A* **2003**, *59*, 351-360.
21. Stixrude, L.; Bukowinski, M. S. T. *Science* **1990**, *250*, 541-543.
22. Brunner, G. O.; Laves, F. *Zeit. Techn. Univ. Dresden* **1971**, *20*, 387-390.
23. Hyde, S. T.; Ramsden, S. in *DIMACS Series in Discrete Mathematics and Theoretical Computer Science* **2000**, *51*, 203-224,.
24. Hyde, S. T.; Ramsden, S. in *Chemical Topology: Applications and Techniques*. Gordon and Breach Science, Amsterdam, **2000**.
25. Corkery, R. *Artificial biomineralisation and metallic soaps*. Ph.D. Thesis, Australian National University, **1998**. Available at <http://hdl.handle.net/1885/46251>
26. Hyde, S. T.; Oguey, C. *Eur. Phys. J. B*, **2000**, *16*, 613-630.
27. Kubota, A.; Caturla, M.-J.; Davila, L.; Stolken, J.; Sadigh, B.; Quong, A.; Rubenchik, A.; Fe, M. D. *Proc. SPIE* **2001**, *108*, 387-390.
28. Kell, G. S. *J. Chem. Eng. Data* **1975**, *20*, 97-105.
29. Fletcher, N. H. *Rep. Prog. Phys.* **1971**, *34*, 913-994.